Procedia Manufacturing

Volume 1, 2015, Pages 287–295

43rd Proceedings of the North American Manufacturing Research Institution of SME http://www.sme.org/namrc

Scanning Speed Effect on Mechanical Properties of Ti-6Al-4V Alloy Processed by Electron Beam Additive Manufacturing

Xiaoqing Wang, Xibing Gong, Kevin Chou

Mechanical Engineering Department

The University of Alabama

Tuscaloosa, AL 35487, USA

Abstract

In this study, mechanical properties in Ti-6Al-4V samples built with the powder-bed electron beam additive manufacturing (EBAM) process over a range of beam scanning speeds were experimentally investigated. Four levels of speed functions were applied to build samples, which were used to prepare the specimens for the nanoindentation test to obtain their mechanical properties. The measured averaged Young's modulus and hardness are about 111.7~119.0 GPa and 5.24~6.52 GPa, respectively. It has been found that the Young's modulus and hardness increase with the increase of scanning speed in EBAM. The scanning surface presents more superior mechanical properties than those from side surface. The mechanical properties are also correlated to the microstructure characterization of EBAM components.

Keywords: Electron beam additive manufacturing, mechanical properties, manoindentation, microstructure, Ti-6Al-4V alloy

1 Introduction

Additive manufacturing (AM), which refer to technologies that create parts through layer-by layer deposition controlled by a computer, has many advantages comparing to traditional manufacturing methods. As one kind of additive manufacturing, electron beam additive manufacturing (EBAM) is one of a few AM technologies capable of making full-density metallic parts and has drastically extended AM applications for direct digital manufacturing of structural components (Murr et al., 2012). In industries, Ti-6Al-4V is the most common titanium alloy being used due to its outstanding mechanical properties, such as high strength, high strength-to-weight ratio, good formability and heat treatability. The EBAM technology on Ti-6Al-4V has wide application in the industry, especially for aerospace components and medical implants.

During the past decade, a lot of research has investigated the mechanical properties of the Ti-6Al-4V parts manufactured by EBAM. Gong et al. (2014a) reviewed the mechanical properties of EBAM

Peer-review under responsibility of the NAMRI Scientific Committee

doi:10.1016/j.promfg.2015.09.026

fabricated Ti-6Al-4V alloy, and found that the EBAM parts have comparable superior mechanical properties to wrought counterparts: high YS and UTS and higher hardness with a lower ductility. Murr et al. (2009a; 2009b) have done extensive research in the field of EBAM Ti-6Al-4V parts, including solid parts and mesh structures. They have studied microstructure, mechanical properties, process parameter, type of defects and quality of parts. Murr et al. (2009b; 2009c) measured the microindentation hardness of the specimen and found that the average value of solid build parts is about 3.6-4.3 GPa, which is very close to the hardness of wrought alloy, while the average mesh structures values is around 4.8 GPa, which is caused by more rapid cooling. Using tensile test and microindentation, Facchini et al. (2009) studied the mechanical properties of Ti-6Al-4V, and the Young's modulus and Vickers hardness of Ti-6Al-4V obtained are 118 GPa and 3.51 GPa, respectively, which are also slight higher than that of wrought and annealed specimens.

It has been reported that EBAM process parameters may have significant effects on the part quality (Gong et al., 2014b). Murr et al. (2009a) studied that variations in melt scan, beam current, and scan speed affect the EBAM built defects such as porosity, which may be used for microstructure-property variations in the final product. The electron beam scanning speed is one of critical parameters to the EBAM process affecting the process condition (Zäh and Lutzmann, 2010). Puebla et al. (2012) and Murr et al. (2009a) studied the effect of build parameters on mechanical properties, and found that and the increase of the scanning speed leads to a decreasing of relatively density and subsequently a decreasing microindentation hardness. The lower hardness could be attributed to the argon gas bubbles trapped in the molten pool at a higher scanning speed.

Nanoindentation is a non-destructive technique used for evaluating mechanical properties from a very small volume of material. It has been widely used to probe the mechanical behavior of Ti-6Al-4V alloy (Xue et al., 2002; Barbieri et al., 2002; Karlsson et al., 2013). However, there have been very few studies on the EBAM-processed Ti-6Al-4V alloy. Ladani and Roy (2013) investigated the Young's modulus of Ti-6Al-4V manufactured by EBAM. Therefore, using nanoindentation test to study mechanical properties of Ti-6Al-4V is the advanced and best method.

The authors' research group has investigated the effects of scanning speed on microstructure, and it is found that the increase of the scanning speed results in the finer microstructure (Gong et al., 2014b). In this work, the specimens were built with four different beam scanning speed level by EBAM. The effect of beam scanning speed on mechanical properties (elastic property and hardness) was investigated with nanoindentation test. Then, taking into consideration of microstructure, the properties of the specimens were evaluated in a comprehensive way.

2 Experiments

The Ti-6Al-4V parts were built in an Arcam S12 EBAM machine at NASA's Marshall Space Flight Center (Huntsville, AL) with the pre-alloyed Ti-6Al-4V powders as the raw material. The major diameter of the powder is around 30 to 50 μm (Gong et al., 2015) and its precise amount of chemical compositions are listed in Table 1 (Gong et al., 2013). With CAD software, the model of the parts with dimension of 60 mm × 5.5 mm × 25mm (L × W × H) was built and imported into the machine. During the fabrication process, the beam size was 0.5 mm and the upper chamber was kept at 7.5×10^{-7} Toll (1 Torr=0.0013157895 atm) to keep the quality of the electron beam, and the fabrication chamber was maintained at a pressure of 7.5×10^{-5} Torr to avoid oxidation of titanium. The parts will be built layer by layer with thickness around 70 um. The whole manufacturing process involves powder spreading, pre-hearting, contour melting and hatch melting. During the melting stages, an electron beam move across the powder-layer surface tracing the model cross-section boundary and then raster-scan through the inside of the contour. The detail of the experiments can be found in the previous studies (Gong et al., 2014a). In an EBAM system, the electron beam is controlled by magnetic deflection coils, which enables the electron beam moves with very high scanning speeds,

e.g., 15 m/s. As to the Arcam EBAM systems used in this study, the actual beam scanning speed can be controlled by the speed function (SF) (Gong et al., 2014b). To investigate the effect of beam speed on mechanical properties, four Ti-6Al-4V parts were built with different SFs (20, 36, 50 and 65), as illustrated in Figure 1.

Table 1: Compositions of Ti-6Al-4V powder (Gong et al., 2013)

Composition	Al	V	C	Fe	O	N	H	Ti
Arcam Ti6Al4V (wt. %)	6	4	0.03	0.1	0.15	0.01	0.003	Bal.

The Ti-6Al-4V specimens used for microstructural observations and nanoidentation test were cut from the built parts with dimension of 11 mm × 5.5 mm×7 mm (L×W×H) by electrical discharge machining, as shown in Figure 2, and were mounted in an epoxy resin and ground using silicon carbide grinding paper from 120 down to 1000 grits with water as coolant, and then polished with diamond suspension down to 0.5 μm. For microstructural analysis, the polished specimens were etched by 1 ml hydrofluoric acid (50 wt. %) and 3 ml (60 wt. %) nitric acid in 7 ml distilled water. Then, the microstructures of the specimens were observed and analyzed with an optical microscope (OM). After the microstructure analysis, the specimens were polished gently again with the same procedures described above. After polishing, the specimens were cleaned by ultrasonic oscillator with distilled water about 1 minute to reduce the influence of surface work hardening.

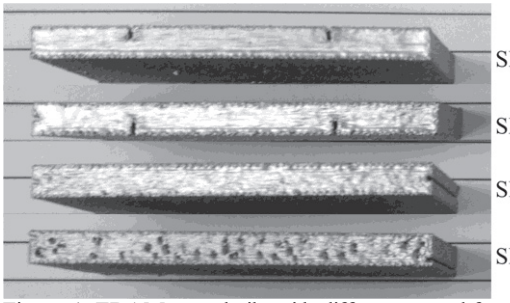

Figure 1. EBAM parts built with different speed functions

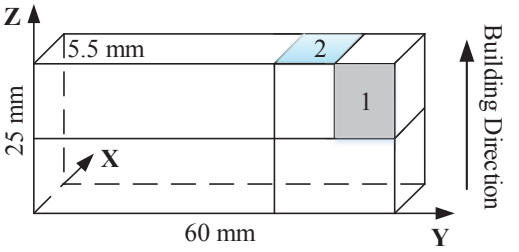

Figure 2. Specimens on Ti-6Al-4V parts

The nanoindentation tests were performed using an in-situ nanomechanical testing system Hysitron Triboindenter™ equipped with a Berkovich tip with radius of 100 nm and an included angle of 142.3°, as shown in Figure 3. The maximum load is 10.0 mN with resolution of 1 nN, and the maximum depth is 20 μm with displacement resolution of 0.04 nm. An open-loop trapezoidal shape load function with maximum load of 5000 μN was applied to the specimens during nanoindentation test, as illustrated in Figure 4. In trapezoidal shape method, the loading force on the indenter increases at a constant load rate until reaching maximum value with a dwell time of 10 seconds, then followed by a constant unload rate until reaching zero. To obtain the precise results, several nanoindenatation tests were conducted on different areas of the specimen. Each run of the tests consisted of a series of 25 indents arranged in a 5 × 5 square pattern with 5 μm spacing between indent locations. The spacing ensured that the stress-strain fields of previous indents did not affect the behavior of any subsequent indent in the series. The sample and tip were allowed to come to thermal equilibrium over 30 min before each test.

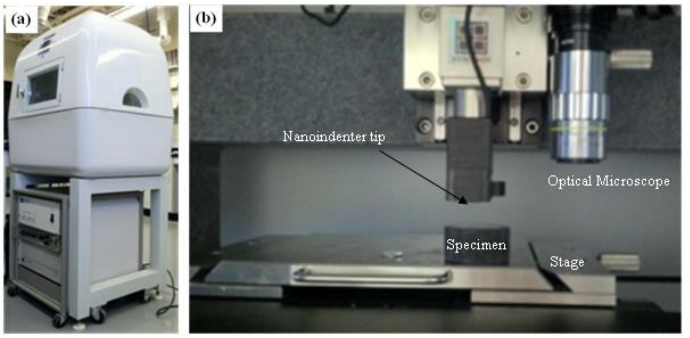

Figure 3. Triboindenter: (a) appearance and (b) nanoindentation setup.

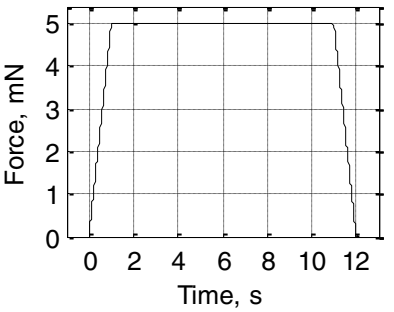

Figure 4. Applied load function

3 Results and discussion

Figure 5 shows an example of the plots of load vs. depth from a small area on the Z-plane sample SF 36 part. The average maximum indentation depth was about 205 nm, and the Young's modulus of the sample could be calculated by:

$$\frac{1}{E_r} = \frac{1-\nu_i^2}{E_i} + \frac{1-\nu_s^2}{E_s}$$

where ν_i=0.07 (Poisson's ratio of indenter), E_i=1140 GPa (Young's modulus of the indenter), ν_s=0.342 (Poisson's ratio of Ti-6Al-4V), E_r=123.39 GPa (reduced Young's modulus of the indenter). Thus the calculated Young's modulus (E_S) of the scanning area. The hardness was obtained as the ratio of the maximum indentation force to the resultant projected contact area evaluated from the shape function of the indenter and the maximum indent displacement.

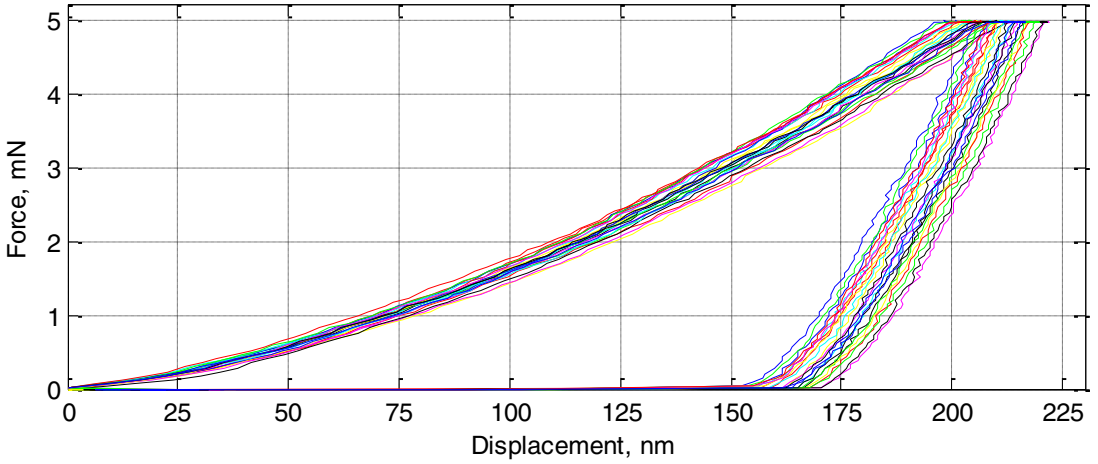

Figure 5. Typical load vs. displacement curves

Figure 6 shows an example of nanoindentation properties from the X-plane (side surface) of an EBAM sample, SF 36. The Young's modulus obtained through nanoindentation test in this study is comparable with mechanical properties of EBAM Ti-6Al-4V alloy from other researchers. As to the experimental results in this study, take the parts built with SF 36 for example, the Young's modulus on the Z-plane (Scanning surface) and X-plane are 116 GPa and 112 GPa, respectively. While the Young's moduli from other researchers are ranged from 108 GPa to 128 GPa, and the average value is around 117.5 GPa, as can be seen from Figure 6(a).

The average hardness on the Z-plane and X-plane of Ti-6Al-4V parts built with SF 36 are shown in Figure 6(b). Murr et al. (2009c) measured the microindentation hardness of the specimen and found that the hardness is between 3.6 GPa and 4.3 GPa, which is very close to the hardness of wrought Ti-6Al-4V alloy, around 4.0 GPa. Similar microhardness of around 4.0 GPa is also achieved from other researchers (Facchini et al., 2009), while the value from other researchers (Baufeld and Van der Biest, 2009) is only 3.1 GPa, which is much smaller. It can be seen from Figure 6 that the hardness obtained from the current study is about 30% higher than the values from literatures. The hardness is about 6 GPa for both Z-plane and X-plane. Different hardness testing methods may lead to the variance of the hardness: the microindentation from other researchers is another different method for hardness test. According to Qian et al. (2005), nanoindentation hardness is 10-30% higher than the micro-indentation hardness for the same samples. The hardness of Ti-6Al-4V obtained through nanoindentation by Li et al. (2008) is between 4-5 GPa. Considering this method factor, the value obtained from this study is just slightly higher than the literature. The Young's modulus for the wrought or cast Ti-6Al-4V is around 120-125 GPa with microhardness around 4-4.2 GPa (Xue et al., 2002; Barbieri et al., 2002). It demonstrates that the mechanical properties of EBAM Ti-6Al-4V alloy are comparable to those from wrought or cast components. The excellent mechanical properties of EBAM parts could be attributed to the fine microstructure and strengthening phase (Gong et al., 2014a). Compared to the wrought or casted specimens, the EBAM parts present much finer microstructure owing to the larger cooling rate during solidification (Gong et al., 2014b). Moreover, the production of martensites because of the very rapid cooling in EBAM. The martensites could work as the strengthening phase in Ti-6Al-4V alloy, and contribute to the improvement of mechanical properties (Gong et al., 2014a).

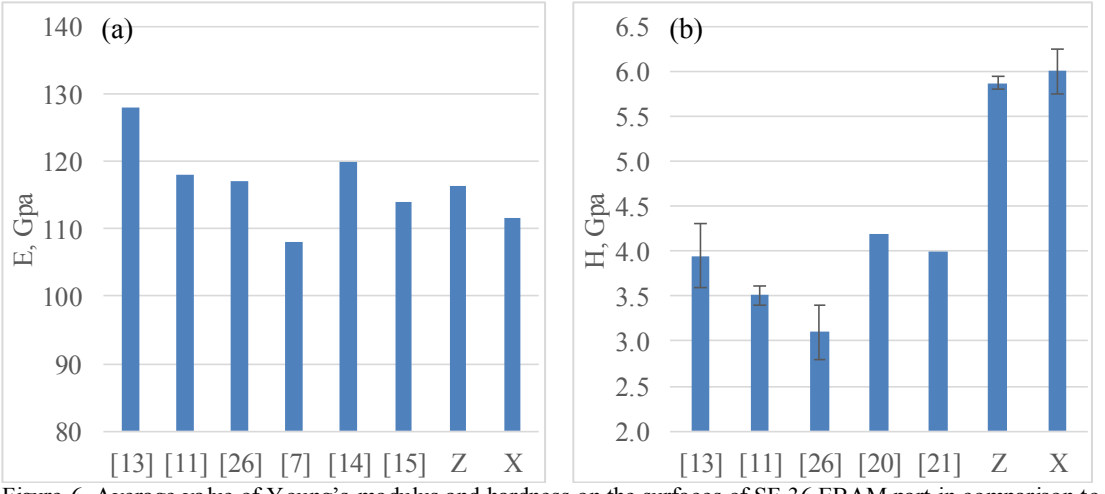

Figure 6. Average value of Young's modulus and hardness on the surfaces of SF 36 EBAM part in comparison to literature: (a) Young's modulus, and (b) Hardness (Note: literature results are microindentation hardness value; "Z" and "X" stand for Z-plane and X-plane)

The results of Young's moduli and hardness of the specimens with different SFs are shown in Figures 7 and 8. Generally, the hardness increases with the increase of the beam scanning speed. However, the exception is the parts built with SF 65, in which the value of hardness shows a lower value. It also can be seen from the Figures 7 and 8 that the measured Young's moduli and hardness at the Z-plane are generally higher than those at the X-plane. The Z-plane presents more homogeneous microstructure compared with the side surface. The fraction of the β is expected to much smaller than that at side surface. During the nanoindentation on the scanning surface, the loading has greater opportunity to apply on the surface of α platelet which is much harder. Another important reason is the

principle of the EBAM, in which the powders are put layer-by-layer. It is evitable that the bonding force on the X-plane is weaker and there are building defects on the side surfaces.

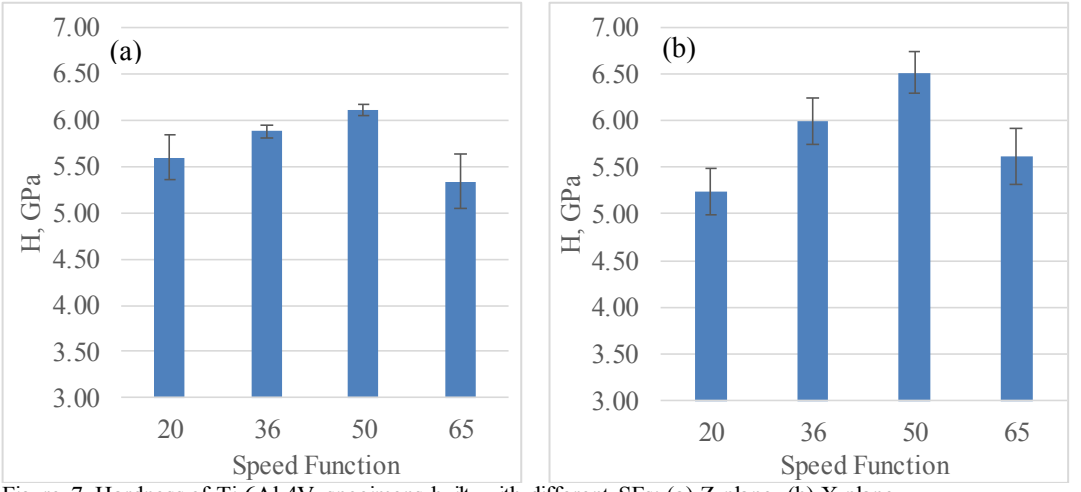

Figure 7. Hardness of Ti-6Al-4V specimens built with different SFs: (a) Z-plane, (b) X-plane

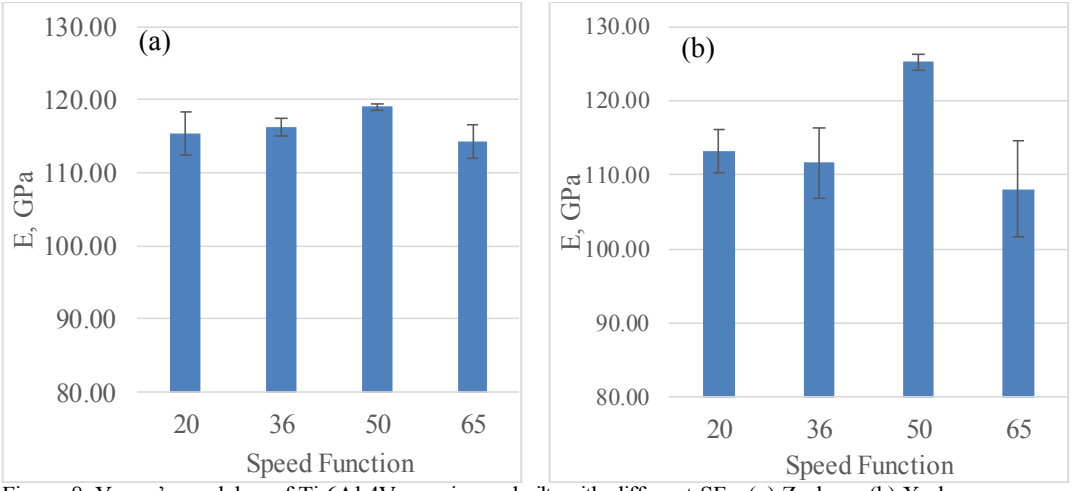

Figure 8. Young's modulus of Ti-6Al-4V specimens built with different SFs: (a) Z-plane, (b) X-plane

To explain the result of the mechanical properties, the microstructure characterizations of the EBAM components are also conducted. From the temperature measurement test, the estimated beam speed values using the method described above were 214 mm/s, 376 mm/s, 529 mm/s and 689 mm/s for SF 20, 36, 50 and 65, respectively. The detailed information of the temperature profiles and melt pool size are discussed in a previous literature (Gong et al., 2014b). Figure 9 shows microstructures from the X-plane (side surface) of for EBAM samples for SF 20 and SF 65. It is obvious that the prior β grains grew along the build direction and across multiple layers in the sample. The columnar prior β grains are typical in high-energy materials processing, and upon rapid cooling from the melt, the growing grains align themselves with the steepest temperature gradients and result in columnar shaped morphology. Another feature in typical EBAM Ti-6Al-4V microstructures is the martensitic phase, α′, which appears as plates, as can be seen in Figure 9. The α′ is transformed from the β phase due to a very high cooling rate. According to Ahmed and Rack (1998), for Ti-6Al-4V, a cooling rate of more than 410 ℃/s. The α′ phase is commonly observed in Ti-6Al-4V alloy subject to rapid solidifications

such as selective laser melting and electron beam welding. The width of the columnar prior β grains was measured in this study. The influence of the scanning speed to the microstructures from the X-plane specimen is shown in Figure 9. Generally, the width of columnar structure decreases with the increase of the scanning speed, 109.7 μm at 214 mm/s vs. 37.1 μm at 529 mm/s. However, the exception is SF 65, in which the width of columnar structure is slightly larger than that of SF 50. For a given beam power, increasing the scanning speed would increase the cooling rate and the thermal gradient, which will form smaller columnar β grains. However, the grain size is generally smaller at a faster cooling rate but the grain size will not reduce if further increase the cooling rate over a certain rate (Ahmed and Rack, 1998; Liu et al., 2014; Ma et al., 2014). On the Z-plane of specimens, the microstructure is characterized by equiaxed grains. The grain size from Z-plane is also listed in Figure 9.

The results of the mechanical properties of EBAM components are related with the microstructure analysis. Generally, with the increase of the beam scanning speed, the microstructure becomes finer and subsequently the components become much stronger according to Hall-Petch's relation. The poor mechanical properties for the SF 65 sample could be attributed to the coarser microstructure than that of SF 50. In addition, the defects in the SF 65, which can also be noticeable at the final build parts' surfaces (Figure 1), also decrease the mechanical properties. The defects SF 65 sample was affected by the small melting pool and melting temperature, this will not only cause some Ti-6Al-4V powder insufficient melt, but also the percentage of pores. This defect will become serious with the increasing of the beam scanning speed.

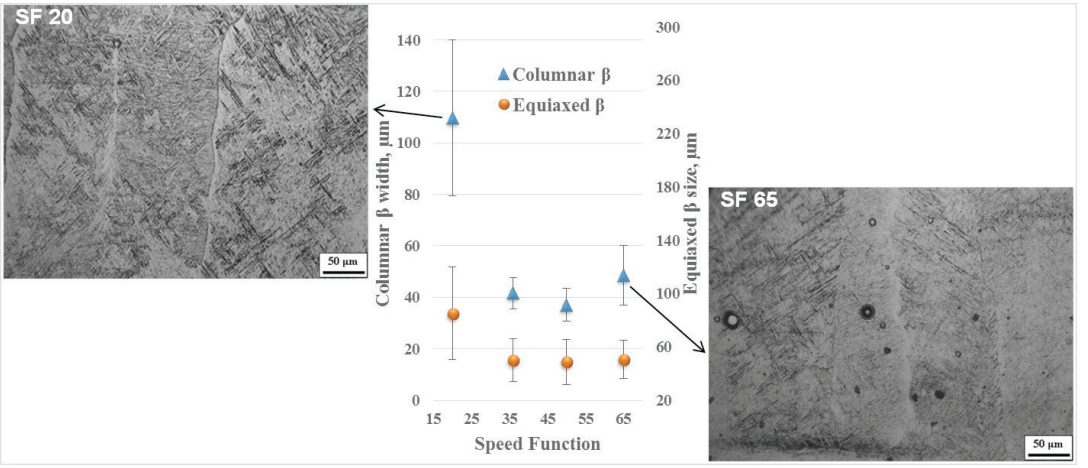

Figure 9. Measured characteristic sizes and microstructures of Ti-6Al-4V parts from samples with various speed functions (Gong et al., 2014b)

4 Conclusion

With the goal of advancing rapid manufacturing of metallic components by deep understanding of fundamental process of EBAM, the present work was conducted to investigate the effects of the beam scanning speed in EBAM by combining microstructure analysis and mechanical properties on Ti-6Al-4V specimens built with four levels of speed function (SF). The major findings are summarized as follows.

a) The Young's modulus of the EBAM Ti-6Al-4V sample is around 111.7~119.0 GPa, and the averaged hardness is about 5.24~6.52 GPa. The mechanical properties are superior or at least comparable to the wrought Ti-6Al-4V alloy.

b) Generally, the Young's modulus and hardness increase with the beam scanning speeds. The more superior mechanical properties for the higher scanning speed could be attributed to the finer microstructure.
c) The scanning surface (Z-plane) has higher strengths (Young's modulus and hardness) than the side surface (X-plane).
d) The optimized mechanical properties could be achieved with the scanning speed between SF 36 and SF 50.

5 Acknowledgements

This research is supported by NASA (award No. NNX11AM11A). XG also acknowledges the AL EPSCoR GRSP for the financial support and XW thanks Dr. Mark L. Weaver for his experimental support.

References

Murr, L. E., Gaytan, S. M., Ramirez, D. A., Martinez, E., Hernandez, J., Amato, K. N., Shindo, P. W., Medina, F. R., Wicker, R. B. (2012). Metal fabrication by additive manufacturing using laser and electron beam melting technologies. *Journal of Materials Science & Technology*, 28(1), 1-14.

Gong, X., Anderson, T., Chou, K. (2014a). Review on powder-based electron beam additive manufacturing technology. *Manufacturing Review*, 1, 1-12.

Murr, L., Gaytan, S., Medina, F., Martinez, E., Hernandez, D., Martinez, L., Lopez, M., Wicker, R., Collins, S. (2009a). Effect of build parameters and build geometries on residual microstructures and mechanical properties of Ti-6Al-4V components built by electron beam melting (EBM). *Proc. of the Solid Freeform Fabrication Symposium*, Austin, TX.

Murr, L., Gaytan, S., Medina, F., Lopez, M., Martinez, E., Wicker R. (2009b). Additive Layered Manufacturing of Reticulated Ti-6Al-4V Biomedical Mesh Structures by Electron Beam Melting. *Proc. of the 25th Southern Biomedical Engineering Conference*, Miami, FL.

Murr, L. E., Esquivel, E.V., Quinones, S. A., Gaytan, S. M., Lopez, M. I., Martinez, E. Y., Medina, F., Hernandez, D. H., Martinez, E., Martinez, J. L., Stafford, S. W., Brown, D. K., Hoppe, T., Meyers, W., Lindhe, U., Wicker, R. B. (2009c). Microstructures and mechanical properties of electron beam-rapid manufactured Ti-6Al-4V biomedical prototypes compared to wrought Ti-6Al-4V. *Materials Characterization*, 60(2), 96-105.

Facchini, L., Magalini, E., Robotti, P., Molinari, A. (2009). Microstructure and mechanical properties of Ti-6Al-4V produced by electron beam melting of pre-alloyed powders. *Rapid Prototyping Journal*, 15(3), 171-178.

Gong, X., Lydon. J., Cooper, K., Chou, K. (2014b). Beam Speed Effects on Ti-6Al-4V Microstructures in Electron Beam Additive Manufacturing. *Journal of Materials Research*, 29(17), 1951-1959.

Zäh, M. F., Lutzmann, S. (2010). Modelling and simulation of electron beam melting. *Production Engineering*, 4(1), 15-23.

Puebla, K., Murr, L. E., Gaytan, S. M., Martinez, E., Medina, F., Wicker, R. B. (2012). Effect of melt scan rate on microstructure and macrostructure for electron beam melting of Ti-6Al-4V. *Materials Sciences and Applications*, 3, 259.

Xue, W., Wang, C., Chen, R., Deng, Z. (2002). Structure and properties characterization of ceramic coatings produced on Ti-6Al-4V alloy by microarc oxidation in aluminate solution. *Materials Letters*, 52(6), 435-441.

Barbieri, F., Otani, C., Lepienski, C., Urruchi, W., Maciel, H., Petraconi, G. (2002). Nanoindentation study of Ti6Al4V alloy nitrided by low intensity plasma jet process. *Vacuum*, 67(3), 457-461.

Karlsson, J., Snis, A., Engqvist, H., Lausmaa, J. (2013). Characterization and comparison of materials produced by Electron Beam Melting (EBM) of two different Ti-6Al-4V powder fractions. *Journal of Materials Processing Technology*, 213(12), 2109-2118.

Ladani, L., Roy, L. (2013). Mechanical Behavior of Ti-6Al-4V Manufactured by Electron Beam Additive Fabrication. *Proc. of the ASME 2013 International Manufacturing Science and Engineering Conference*, Madison, WI.

Gong, X., Lydon, J., Cooper, K., Chou, K. (2015). Characterization of Ti-6Al-4V powder in electron beam melting additive manufacturing. *International Journal of Powder Metallurgy*, 51(1), 1-10.

Gong, X., Chou, K. (2013). Characterization of Sintered Ti-6Al-4V Powders in Electron Beam Additive Manufacturing. *Proc. of the ASME 2013 International Manufacturing Science and Engineering Conference*, Madison, WI.

Baufeld, B., Van der Biest, O. (2009). Mechanical properties of Ti-6Al-4V specimens produced by shaped metal deposition. *Science and Technology of Advanced Materials*, 10(1), 015008.

Qian, L., Li, M,, Zhou, Z,, Yang, H., Shi, X. (2005). Comparison of nano-indentation hardness to microhardness. *Surface and Coatings Technology*, 195(2-3), 264-271.

Li, R., Riester. L., Watkins, T. R., Blau, P. J., Shih, A. J. (2008). Metallurgical analysis and nanoindentation characterization of Ti-6Al-4V workpiece and chips in high-throughput drilling. *Materials Science and Engineering: A*, 472(1-2), 115-124.

Ahmed, T, Rack, H. (1998). Phase transformations during cooling in α+β titanium alloys. *Materials Science and Engineering: A*, 243(1), 206-211.

Liu, S., Liu, W., Harooni, M., Ma, J., Kovacevic, R. (2014). Real-time monitoring of laser hot-wire cladding of Inconel 625. *Optics & Laser Technology*, 62(0), 124-134.

Ma, J., Kong, F., Liu, W., Carlson, B., Kovacevic, R. (2014). Study on the strength and failure modes of laser welded galvanized DP980 steel lap joints. *Journal of Materials Processing Technology*, 214(8), 1696-1709.